REPORT DOCUMENTATION PAGE

Form Approved
OMB No. 0704-0188

1. REPORT DATE *(DD-MM-YYYY)*	2. REPORT TYPE	3. DATES COVERED *(From - To)*
13-05-2009	Final Technical Report	15-02-2007 to 30-11-2008

4. TITLE AND SUBTITLE
Phonon Avoided and Scalable Cascade Lasers (PASCAL)

5a. CONTRACT NUMBER

5b. GRANT NUMBER
N000140710564

5c. PROGRAM ELEMENT NUMBER

6. AUTHOR(S)
Hooman Mohseni

5d. PROJECT NUMBER

5e. TASK NUMBER

5f. WORK UNIT NUMBER

7. PERFORMING ORGANIZATION NAME(S) AND ADDRESS(ES)
Northwestern University
633 Clark Street
Evanston, IL 60208

8. PERFORMING ORGANIZATION REPORT NUMBER
CNV0051599-final report

9. SPONSORING/MONITORING AGENCY NAME(S) AND ADDRESS(ES)
Office for Naval Research
875 North Randolph Street
Arlington, VA 22203-1995

10. SPONSOR/MONITOR'S ACRONYM(S)
ONR

11. SPONSOR/MONITOR'S REPORT NUMBER(S)

12. DISTRIBUTION/AVAILABILITY STATEMENT
Approved for public release, distribution unlimited.

13. SUPPLEMENTARY NOTES

14. ABSTRACT
In the DARPA-EMIL program, we investigated and developed a novel process of forming such QD applying lateral electric field. This method doesn't change the structure permanently as in chemical processes and it is much more uniform compared to other methods. We implemented QDs on a cascade laser structure and formed phonon avoided scalable quantum cascade laser (PASCAL). We have implemented self-assembled nanosphere lithography technique to form uniform array of quantum dot pattern. This novel technique has been published in several peered reviewed journals and became the cover story of NanotechnologyDecember, 2007 issue. We also designed an "injectorless" QCL design, with extremely short (about half of conventional) gain periods to be implemented with the PASCAL design. Its improved thermal performance have been recently published in Applied Physics Letter February,2009.

15. SUBJECT TERMS

16. SECURITY CLASSIFICATION OF:			17. LIMITATION OF ABSTRACT	18. NUMBER OF PAGES	19a. NAME OF RESPONSIBLE PERSON
a. REPORT	b. ABSTRACT	c. THIS PAGE			19b. TELEPHONE NUMBER *(Include area code)*
U	U	U		20	

Final Technical Report

EMIL-PASCAL

Name of Grantee:	**Northwestern University**
For Period:	**February15th, 2007 to November 30th 2008**
Contract Title:	**Phonon Avoided and Scalable Cascade Lasers (PASCAL)**
Prime Grant #:	**N000140710564**
Report Recipients:	**Dr. Mihal Gross**

A. Summary

Although the general rules of designing the cascade structure are well understood, it is becoming increasingly difficult to improve its wall-plug efficiency further by just redesigning its cascade layer structure. Because, the ultimate performance of QCL still faces the fundamental limitation of the non-radiative LO phonon relaxation, which is faster compared to radiative process. It is well known that the radiative problem can be overcome by converting the quantum-well (QW) active region of QCL into a quantum-dot (QD) array. Several methods like applying magnetic field, etch-re growth,and self-assembly methods have been tried to form QDs. In DARPA-EMIL program, we investigated and developed a novel process of forming such QD applying lateral electric field. This method doesn't change the structure permanently as in chemical processes and it is much more uniform compared to other methods. We implemented QDs on a cascade laser structure and formed phonon avoided scalable quantum cascade laser (PASCAL).

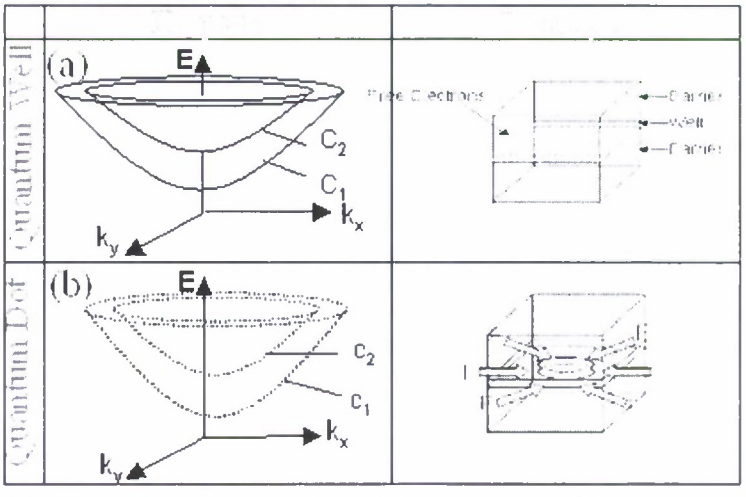

Figure 1- (a) Schematic band diagram of QW structure where LO phonon can relax between any two points of the subband planes (b) Subband states become quantized in QD structure due to confinement and it limits LO phonon relaxation

Energy states in a QW structure are naturally quantized along the crystal growth direction. Applying lateral electric field results in confinement in the plane perpendicular to the growth direction and thus forming 3d electrically confined electronic wavefunctions. We have implemented self-assembled nanosphere lithography technique to form

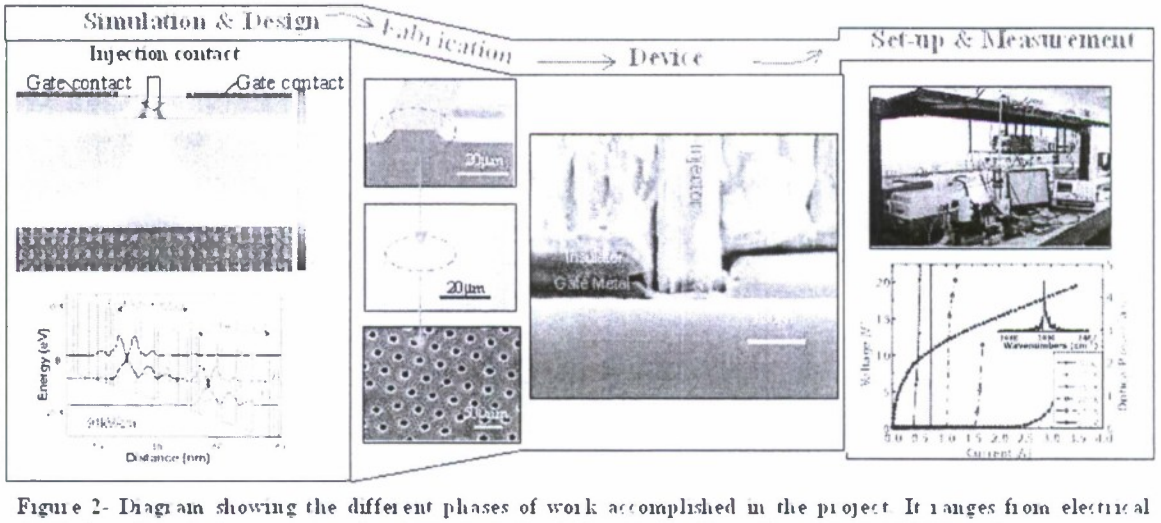

Figure 2- Diagram showing the different phases of work accomplished in the project. It ranges from electrical simulation of the device structure, band structure simulation, device fabrication, set-up building and measurement

uniform array of quantum dot pattern. This novel technique has been published in several peered reviewed journals and became the cover story of *Nanotechnology December, 2007* issue. We also designed an "injectorless" QCL design, with extremely short (about half of conventional) gain periods to be implemented with the PASCAL design. Its improved thermal performance have been recently published in *Applied Physics Letter February,2009*. Detialed project summary will be described below.

B. Summary of Accomplishments

1. ***Modeling:*** Final structure of PASCAL-QCL, with electrically tunable quantum dots in the active region, was designed and optimized using our 3D electrical and optical simulation stools. Important parameters such as thickness, doping density of different layers of PASCAL (upper cladding, Active and lower cladding) were optimized for high electronic confinement and low optical loss. The quantum states and electron wavefunctions were calculated from the simulated potential distribution. These simulations showed strong depletion of electrons outside the confinement-region due to reverse biasing, thus forming a funnel shape structure in the active region, which is physically analogous to quantum dot (QD). Deposition of a thin layer of silicon dioxide between InGaAs top cladding and aluminum contact was proposed and proved to significantly reduce the optical loss. An Injectionless PASCAL-QCL structure was further designed which has very low voltage defect

2. ***Growth:*** Wafers of PASCALs were grown with strain-compensated layers using Metal-Organic-chemical-vapor-deposition (MOCVD). X-ray diffraction reflects excellent agreement to the designed layer thickness and composition, as well as high crystalline quality. Other characterizations including photoluminescence and SIMS showed very good epitaxial quality.

3. ***Processing:*** Processing has been focused on 5 different devices – (a) PASCAL (b) Injectionless PASCAL (c) double channel standard and injectorless QCL. 7 masks process have been designed to form PACAL device. Several issues like RIE etching of hole, developing time of lithography, anodization of hole side wall, substrate heating with e-beam evaporation, formation of burned photoresist film have been solved.

4. ***Characterization:*** The output power and applied voltage versus current (L-I-V) characteristics of conventional QCL laser was obtained with the mounted device placed on a temperature-controlled cold finger of a nitrogen-cooled cryostat. Power measurements were performed on various laser devices up to 300K, in pulsed mode with a pulse width of 100ns and a repetition frequency of 1KHz. We also studied the spectral characteristics of Fabry-Perot QC-Laser working in pulsed mode at 300K with a current pulse of width 300ns using Nicholet 8700 FTIR time-resolved-step-scan with a maximum resolution of $0.125cm^{-1}$.

B.1. Modelling

A 3D finite-element-method (FEM) based model with cylindrical symmetry was custom developed using *Comsol multiphysics* to evaluate the electrical performance of the device and a 2D finite- element time domain (FDTD) based optical simulator *Lumerical* to evaluate the waveguide loss and modal confinement. The electrical model has full 3-D simulation capability and 2-D cross-section modeling capability with cylindrical symmetry. It incorporates several non-linear effects in to consideration. We also collaborated with the group of Prof. M.C. Amann at TU Munich to verify the validity of electrically forming 3d electrical confinement and got excellent results supporting our previous results. Band structure for Quantum Cascade design was simulated using *Comsol Multiphysics*. We also used *Nanonext,* which used 8-band k-p model to solve band structure. Thermal performance of the waveguide was simulated using *Comsol Multiphysics.*

The whole gamut of simulations was performed over different phases over the 18 months project and the table below describes it.

Simulation Tasks		Months					
		3	6	9	12	15	18
A1	Develop the simulation structure using *Comsol Multiphysics*						
A2	Doping density optimization						
A3	Thickness optimization of different layers						
A4	Leakage and injection current estimate						
A5	Wavefunction deformation in 3d confinement						
A6	Injectorless QCL design						
A7	Injectorless PASCAL design						
A8	Electrical simulations using *Nanonext*						
A9	Electrical Simulation by TU Munich						
A10	Thermal simulation of waveguide structure						
B1	Waveguide loss & modal confinement estimate						
B2	Optical simulations for Super Lens Litho						
B3	Optical simulations by TU Munich						

Task Duration → Task Connection Task revisit

Table 1 – It shows the electrical and optical simulations performed over the 18months of EMIL-DARPA program in different phases.

A.1.1 Electrical Simulations

In principle, modeling of PASCAL is a very demanding task since it is a true 3-dimensional structure. Semiconductor double-hetero (DH) structure naturally confines e^- along

one crystal axis. The planar confinement is further provided by the electron depletion due to reverse biasing in PASCAL.

Parameters such as active layers thickness, doping concentration of different layers, doping concentration and thickness of cladding layers of PASCAL were designed for effective lateral confinement of electrons. Parameters were varied to reach an optimum structure with high electron confinement as well as low optical loss. The thickness of different layers of active/injector region quantum wells was kept the same as one standard Quantum Cascade Laser (QCL) structure. Thus, PASCAL design can give scalability to any QCL irrespective to its active/injector region design.

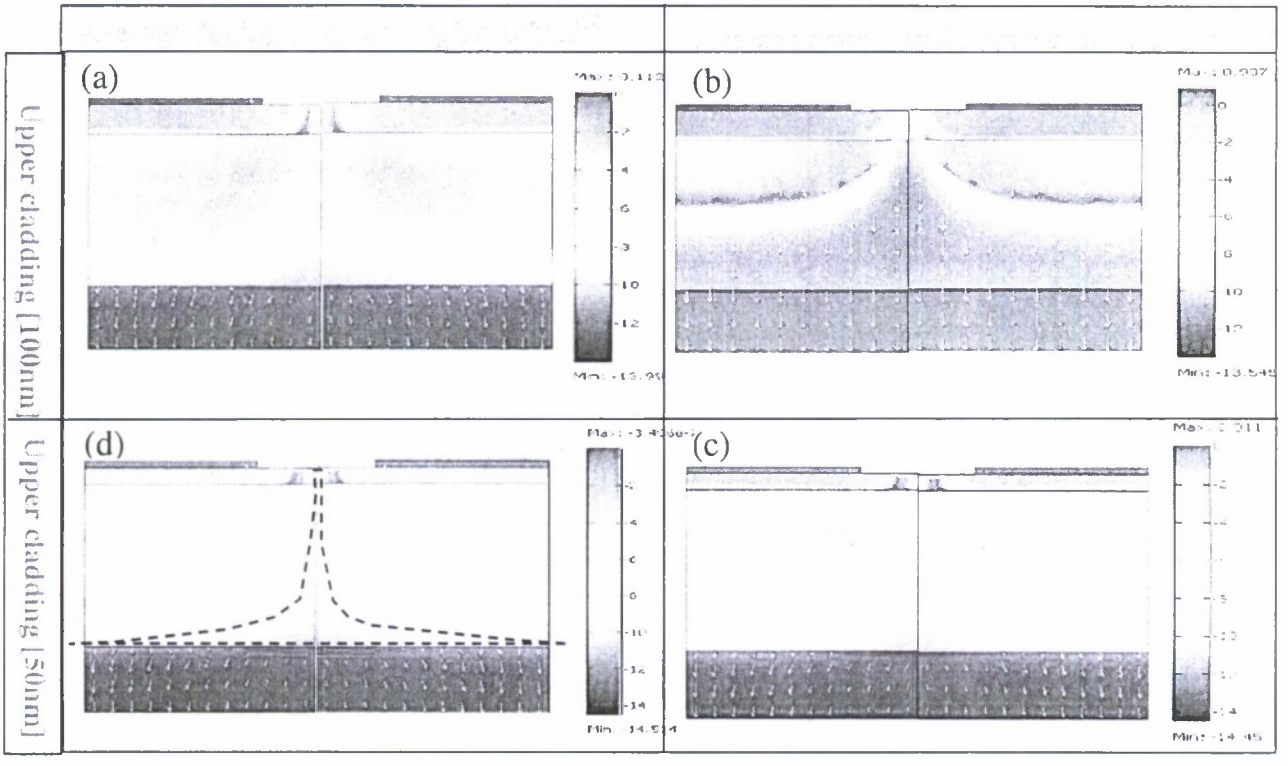

Figure 1 - Electrical simulations have been performed with varying doping density, layer thickness to find the optimized design which has good 3d electron confinement. (a), (b), (c), (d) show a snapshot of such series of simulation designs which has performed with an applied injection voltage of 4.5 V and gate voltage of – 4.5 V. The domain color bar shows the plot of log (n/N), where n is the free electron density and N is intrinsic electron density. Design (d) is used for growth and its confinement has been shown using black dotted line.

Doping density plays a pivotal role in confinement as been shown in Figure 1. Average doping density in the active/injector region was reduced in the PASCAL design structure compared to standard QCL. The optical loss of PASCAL structure with different thickness of upper cladding was compared. Upper cladding thickness of 50nm with doping density of 3.0×10^{16} cm^{-3} had been estimated to optimize the electron confinement and modal loss. Parameters like change of refractive index with doping, thermal conductance of InGaAs upper cladding have also been considered in deciding parameters for the electrical simulations.

We also collaborated with the group lead by Prof. M. C. Amann at TU Munich to discuss the idea of electrical confinement using lateral electric field. They simulated on the same design found by the simulations shown before, and found significant electrical confinement as shown in Figure 2.

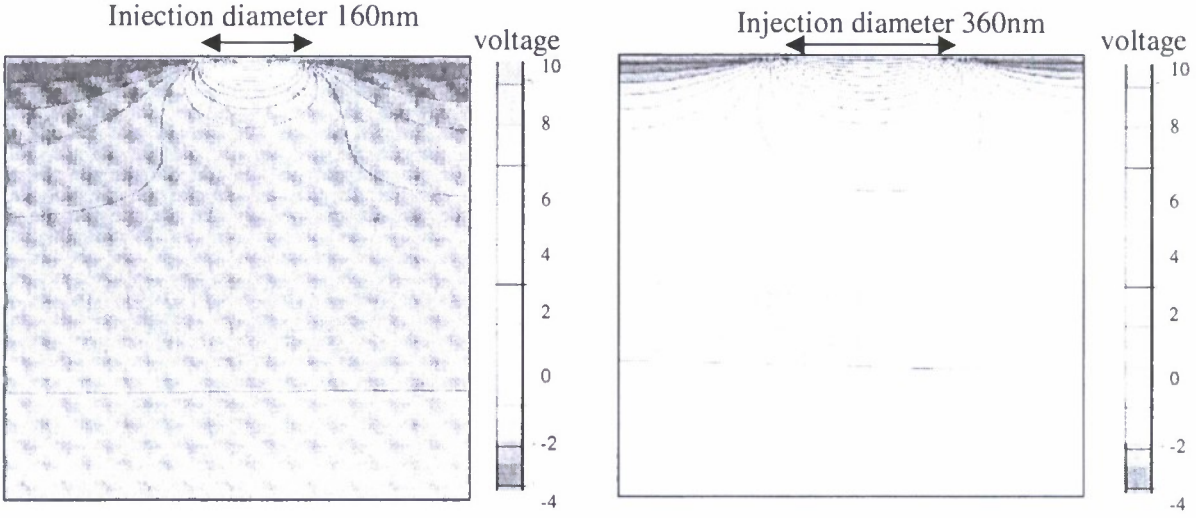

Figure 2 – Electrical simulations performed by TU Munich, Germany to show the electrical confinement using lateral field. They varied the injection diameter to see the penetration depth of the field.

The wavefunctions of the confined structure were evaluated by solving scrodinger equation. Simulations also found that the electron energy levels can be separated u to ~ 50meV, while longitudinal phonon energy is ~ 30meV. Thus such mechanism can reduce the non-radiative LO phonon relaxation.

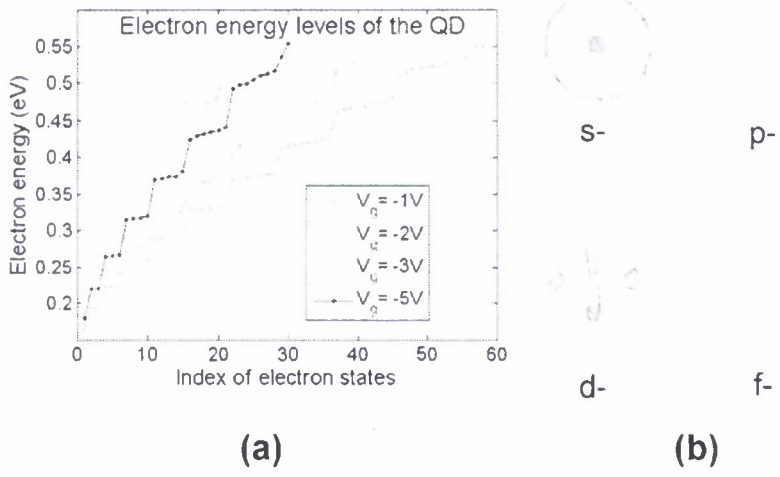

Figure 3 - (a) Shift in adjacent electronic energy levels by electrical 3 d confinement. (b) Shape of the different electronic wavefunctions for the system.

An injectorless-QCL was designed with $In_{0.65}Ga_{0.35}As/In_{0.385}Al_{0.615}As$ strain-compensated layer sequence of one period as follows, starting with undoped $In_{0.65}Ga_{0.35}As$ quantum well 6.5/*1.0*/5.0/*1.3*/**4.0**/**2.8**/**2.8**/*1.4*/1.2/*1.0*, with bold layers are averagely doped to $2.3x10^{16}$ cm^{-3} and $In_{0.365}Al_{0.635}As$ barrier layers are printed in italics. All layers are grown on N-doped InP substrate (Si, $2.0x10^{17}$ cm^{-3}). The injectorless structure has 60 active regions sandwiched between 500nm n-doped $In_{0.53}Ga_{0.47}As$(Si, $5.0x10^{16}$ cm^{-3}). The upper cladding consists of a 2.5μm n-InP (Si, $1.0x10^{17}$ cm^{-3}), followed by 800nm n-doped $In_{0.53}Ga_{0.47}As$(Si, $5.0x10^{18}$ cm^{-3}) and highly doped 200nm contact layer of n-doped $In_{0.53}Ga_{0.47}As$ whose doping is $3.0x10^{19}$ cm^{-3}.

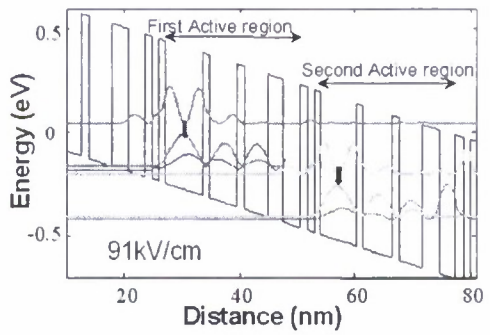

Figure 4 - Conduction band diagram of $In_{0.365}Al_{0.635}As/In_{0.65}Ga_{0.35}As$ injectorless quantum cascade laser (I-QCL) under a positive bias corresponding to an applied voltage of 91 kV/cm. Two successive active regions are shown and the black thick arrow indicates the lasing transition at 184 meV

A.1.2 Optical Simulations

Propagation loss and effective refractive index were calculated for varying thicknesses of metal film and semiconductor layers for PASCAL design structure. Initially, a structure with n-InP as cladding layer was simulated, which showed significant propagation losses To further confine the optical mode we considered using a thin film of low refractive index silicon dioxide (SiO_2) or silicon nitride (Si_3N_4) instead of n-InP to decrease the propagation loss. The main concern was that whether an effective depletion can be achieved with the metal-insulator-semiconductor (MIS) structure or not. Electrical simulations were performed with p-doped InP layers, which was closely analogous to the performance of insulating oxide or nitride in terms of forming depletion.

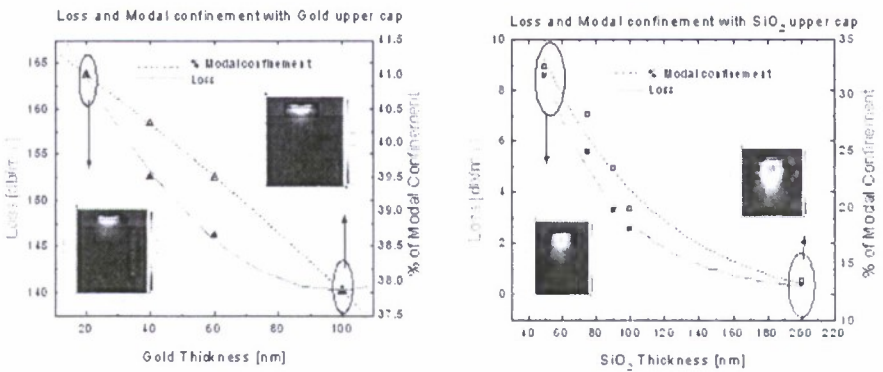

Figure 5 - Optical loss of PASCAL structure with varying thickness of direct metal contact metal contact through micro-hole with a oxide layer above InGaAs upper cladding.

B.2. Growth

PASCAL structure was grown on n^+ InP substrate (Si, $3x10^{18}$ cm^{-3}) by MOCVD. Unlike the conventional QCL structure, the device consists of 10 active/injector stages (0.51μm), each stage containing a 4 quantum-well (QW) active region. Average doping of active region was reduced to $1.5x10^{16}$ cm^{-3} compared to $2x10^{17}cm^{-3}$ for conventional QCL. The active region is sandwiched between InGaAs thin (50nm) upper cladding and thick (330nm) lower cladding with doping density of $3x10^{16}cm^{-3}$. Active region consists of strain-compensated $In_{0.44}Al_{0.56}As/In_{0.6}Ga_{0.4}As$. Double crystal x-ray spectroscopy was performed to verify the thickness of different layers of quantum wells [

Figure 6].

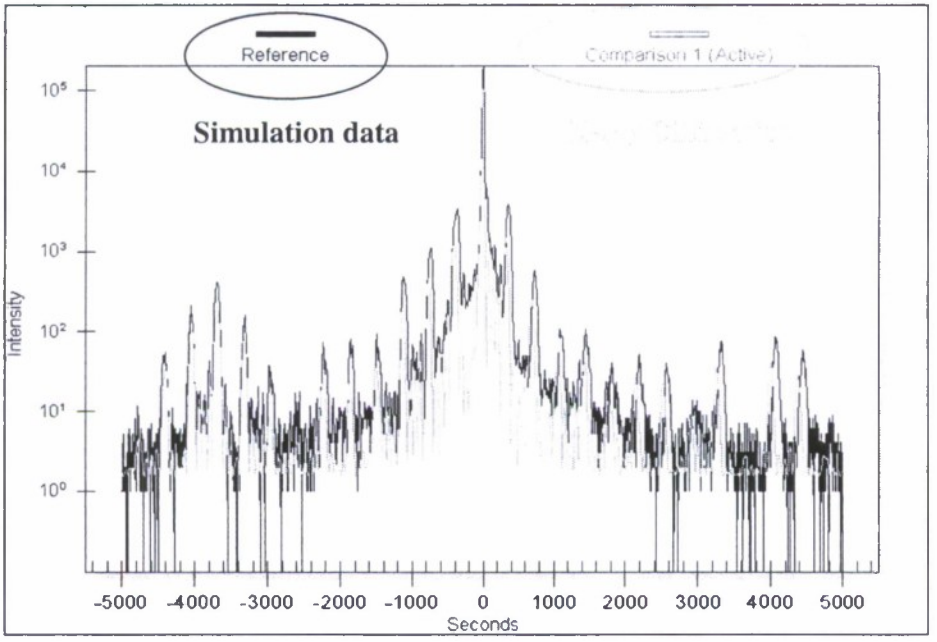

Figure 6 - X-ray diffraction of PASCAL test structure is compared with simulation

A conventional QCL structure was also grown on an n^+ InP substrate by MOCVD in a single growth-step. The device consists of similar 30 active/injector stages as with 4 quantum-well (QW) active region having an average n-doping (Si, $2x10^{17}cm^{-3}$). It is sandwiched between thick upper and lower cladding. The x-ray diffraction has showed an excellent match with the proposed layer thickness of the device .The excellent quality of the sample is further supported by the photoluminescence spectrum and SIMS.

B.3. Processing

The fabrication can be categorized in two separate parts –

(a) Convetional quantum cascade laser

(b) PASCAL fabrication

We had processed 2 wafers of conventional QCL, 2 wafers of injectorless QCL, 4 wafers of PASCAL and 4 wafers of I-PASCAL.All wafer were cleaved into 4 parts. A QCL wafers has 5-6 steps of processing and it takes about a week to finish fabrication. On the other hand PASCAL has 38 steps of fabrication, with extremely intricate steps of fabrication and it took more than a month for a wafer fabrication.

We designed a 6 photolithographic masks process to fabricate such dual contact QCL device. It also involved a maskless photolithographic process called super lens lithography to form such "quantum dots" but at low cost with higher uniformity. Different steps of PASCAL processing were revisited and optimized. Though we couldn't yield a working PASCAL device, we solved and discovered many significant recipes for semiconductor fabrication.

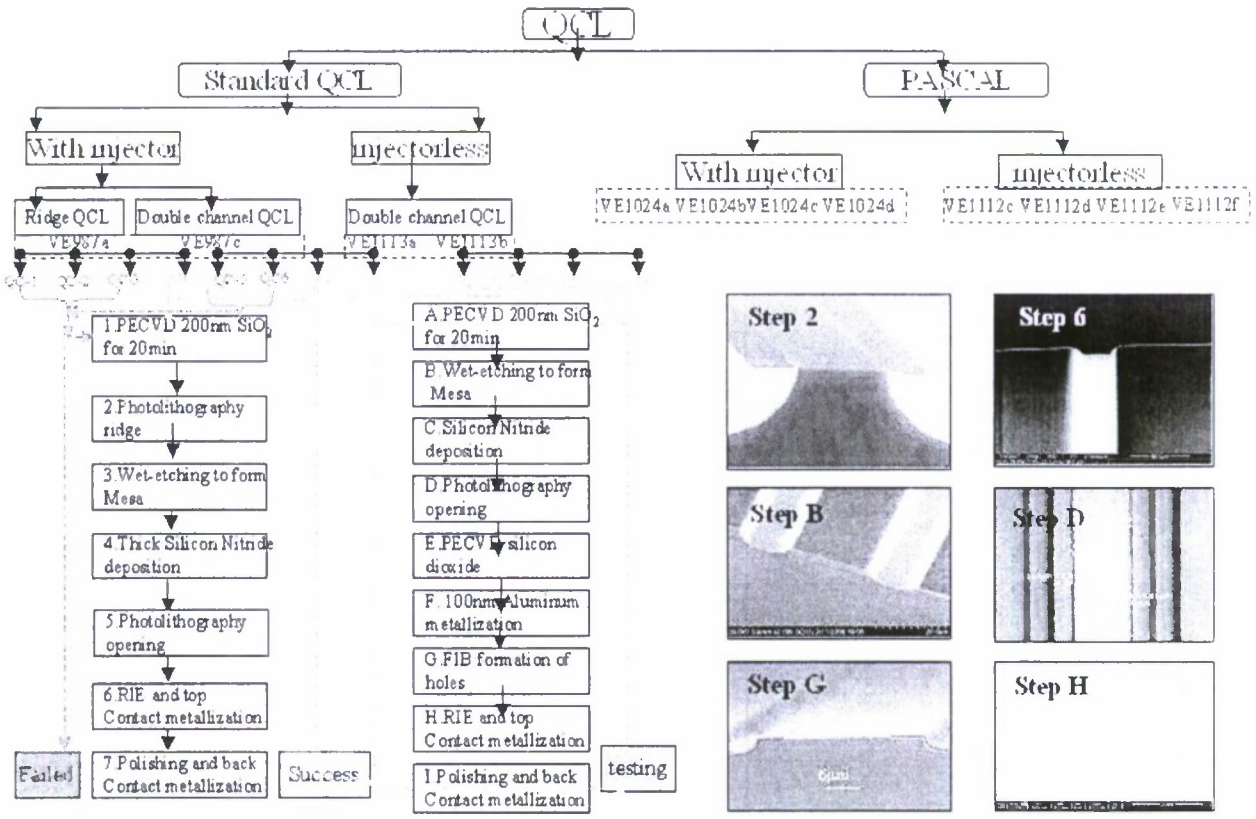

Figure 7 – Schematic diagram of conventional and injectorless QCL samples and fabrication steps, which were performed during the 18 months DARPA-EMIL program.

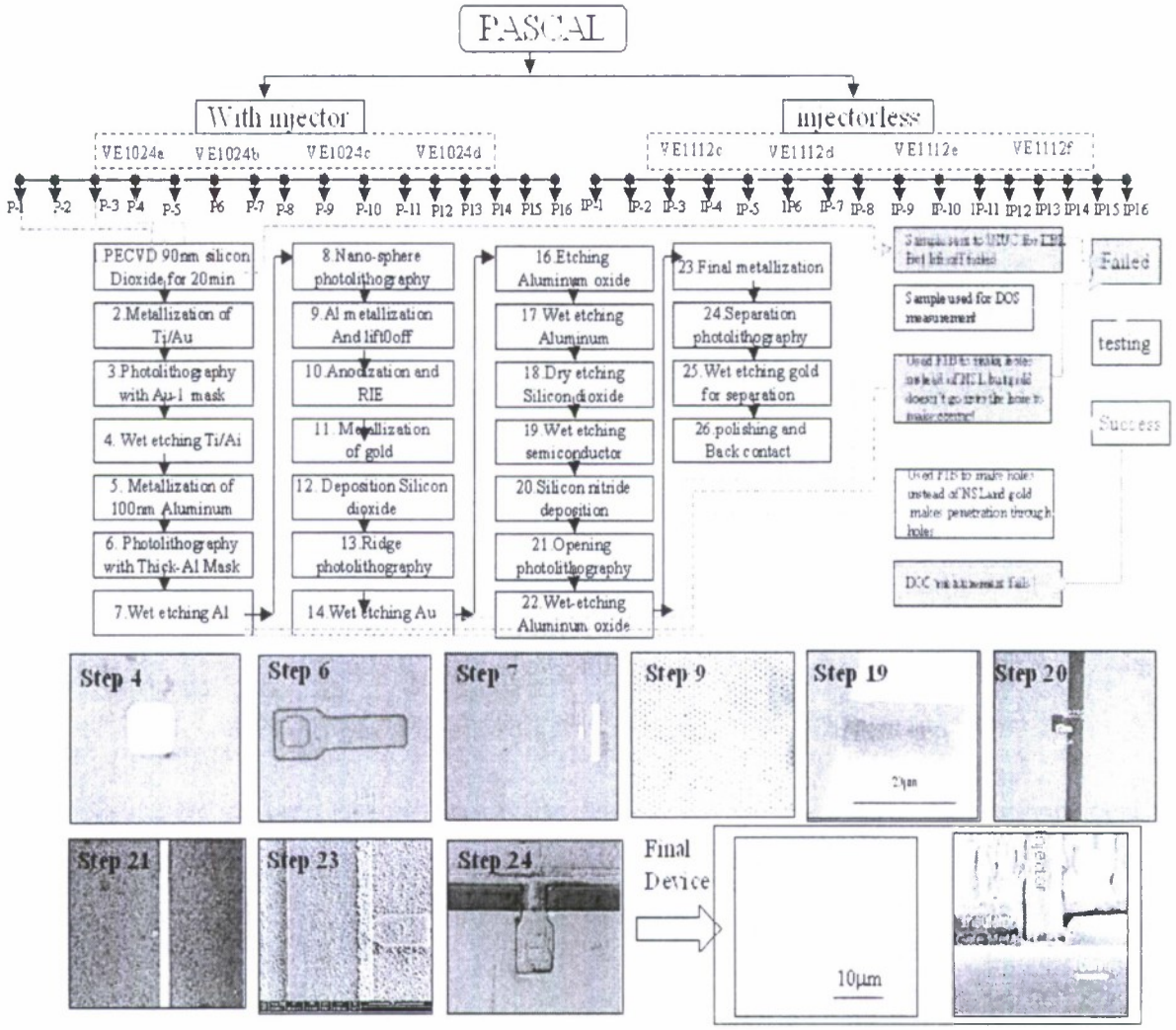

Figure 8 - Schematic diagram of PASCAL and I-PASCAL samples and a snapshot of the fabrication steps, which were, performed during the 18 months DARPA-EMIL program.

12 steps processing flow has been designed to fabricate PASCAL structures. 6 required photolithographic masks have been fabricated .The processing steps and the layout at each step have been shown in Figure 10.

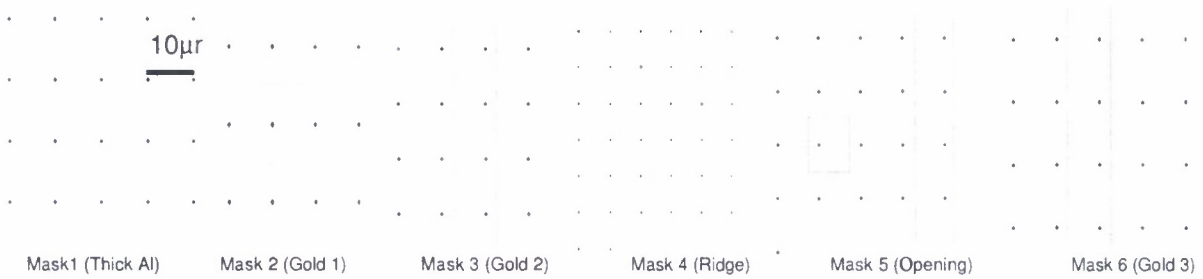

Figure 9 - Cross-section of each mask layouts of PASCAL processing

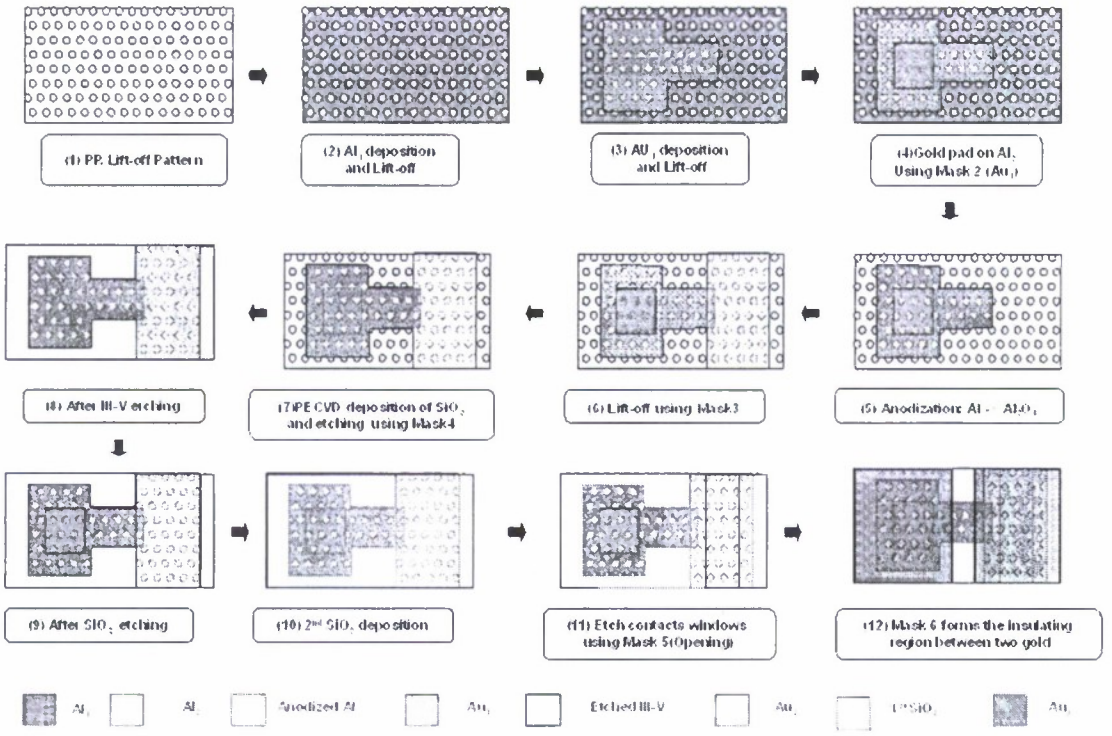

Figure 10 - the process flow designed to fabricate PASCAL

PASCAL fabrication is extremely challenging task and insurmountable amount of time had been spent its fabrication process as well as finding the optimized recipes for each steps.

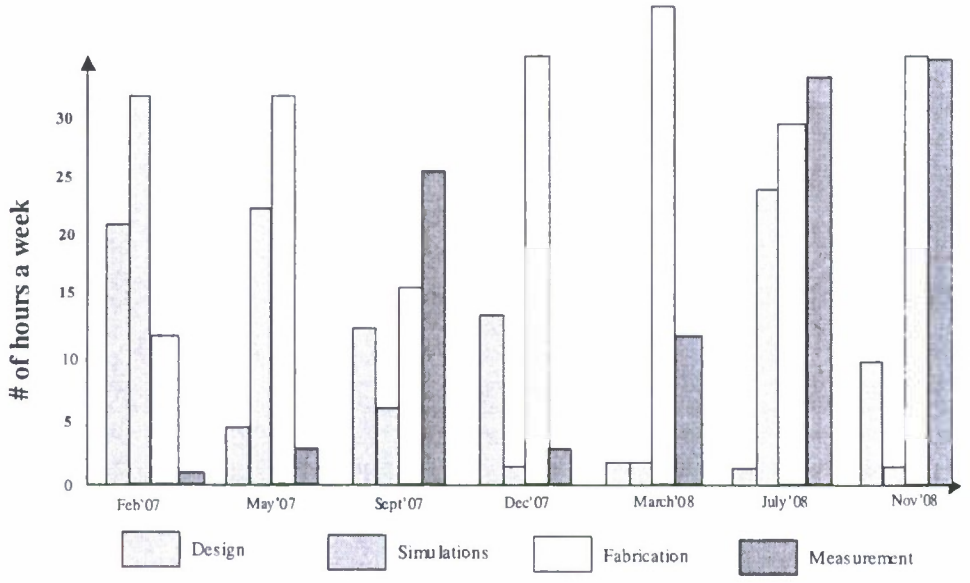

Figure 11 – Schematic showing a rough estimate of the # of hours spend on discussions, simulations, fabrication measurement over the whole DARPA-EMIL program.

A.3.1 Super Lens Lithography

The most important fabrication step to form such quantum dots is to form uniform array of hole pattern where each hole is used to form the injection contact. We used a maskless photolithographic technique called Super Lens Lithography (SLL) for this purpose. Super Lens Lithography technique applies the super focusing ability of spherical silica or polystyrene spheres into lithography technique. It is a maskless technique but can generate subwavelength nanopatterns (~200nm) under normal UV lamp (λ~400nm), which saves a lot of time and cost on fabrication of photo-masks and updating new exposure instrument with lower exposure light wavelength. An interesting fact is found that the size of the microspheres used has almost no influence on the nanopatterns generated, which helps avoid the size un-uniformity caused by the size difference of microspheres. The nanopatterns generated are also tunable using different wavelength of light source and different exposure and development time. Different parameters, such as the materials and the diameter of the micro-spheres, different UV light wavelengths, have been simulated to get an optimized result for the fabrication of nano-patterns. We have confirmed that both silica and polystyrene micro-spheres can be used as the super-lens for UV light. Different diameters of micro-spheres have almost no effect on the nano-feature sizes (but will change the periods of the array [Figure 14]. Using smaller wavelengths, even smaller nano-features can be generated.

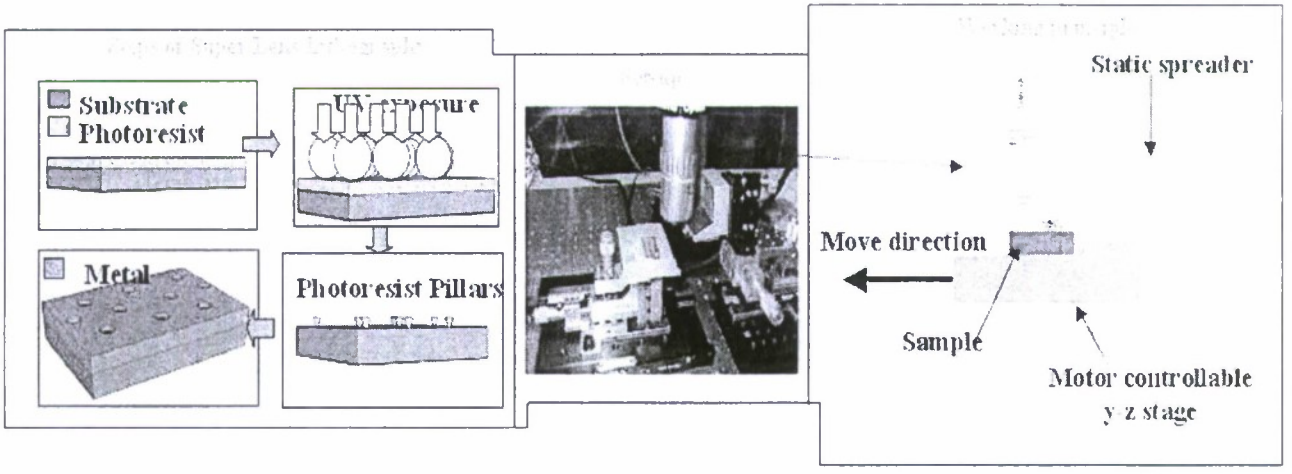

Figure 12 – (a) The schematic diagram of the different steps of formation of nano holes using SLL. (b) Set-up developed in our lab for SLL (c) Schematic diagram of the set-up

We fully developed the mask-less nanolithography technique. The SEM micrographs show that highly uniform nanoholes and nanopillars array can be generated by the technique. The technique is a tunable process and can generate nanopatterns with different sizes and periods. Microspheres was assembled as a monolayer on top of photoresist as big as cm^2 using our lab-made setup, which is shown in Figure 12.Nanopillars of photoresist was generated by the technique and we produced a large area of high uniform nanoholes perforated in Al films, which is a big step towards making quantum dot intersubband cascade lasers, by lift-off.

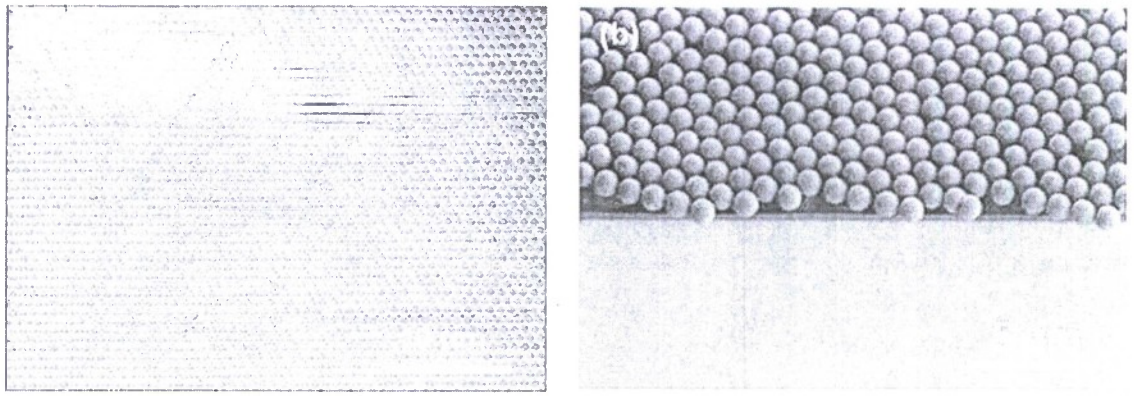

Figure 13 - (a) a large area of monolayer of silica spheres standing on top of photoresist; (b) the enlarged side view of the silica spheres on photoresist

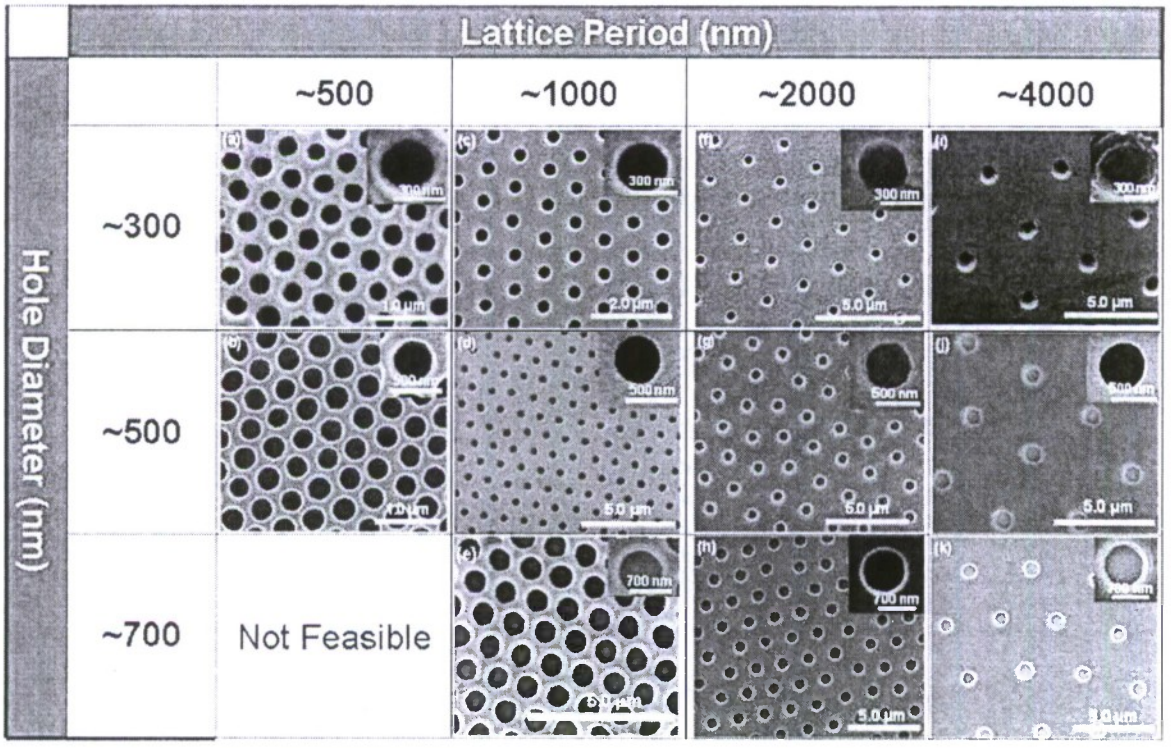

Figure 14 - SEM images series showing nanoholes generated with different diameters and periods

A.3.2. Issue of nano-pillar formation during SLL

During the nanopillars of photoresist formation, we always found a very thin layer of photoresist on the substrate, which was understandable, since the nanopillars generated had such a high aspect ratio. We could do the lift-off to form the nanoholes. However, this thin layer of photoresist would affect our process steps later, which I will discuss. To get a clean surface, we did more experiments to calibrate the development time and optimized the exposure time. When using e-beam evaporator to deposit Al for making lift-off, we slowed down the evaporation rate with several breaking times, and kept the beam of the evaporation as vertical as possible.

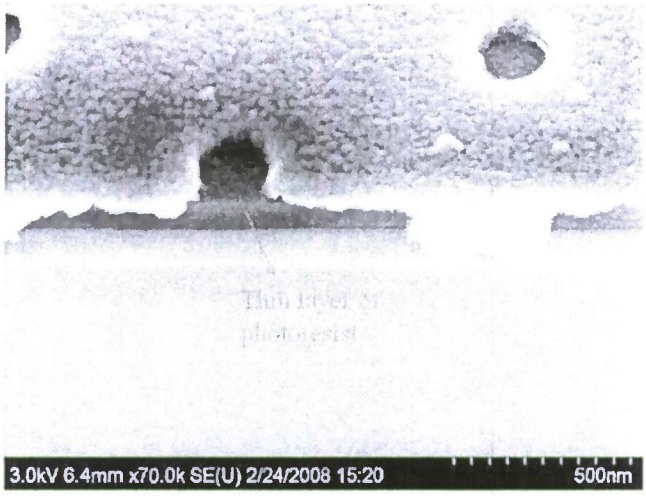

Figure 15 - SEM images show the thin layer of photoresist

A.3.3. Issue with Anodization

Anodization with gold pads on top of Al: we found that when we first put the thick Al and then put the second mask for gold pads, our anodization always failed and the gold pads disappeared. The reason was that all the anodization current would flow to gold pad rather forming aluminum oxide when there was the short circuit from the electrolyte to the gold. Our solution was we first formed gold pad and then formed thick aluminum pad on top of it. And finally we would open the gold pad by etching the aluminum.

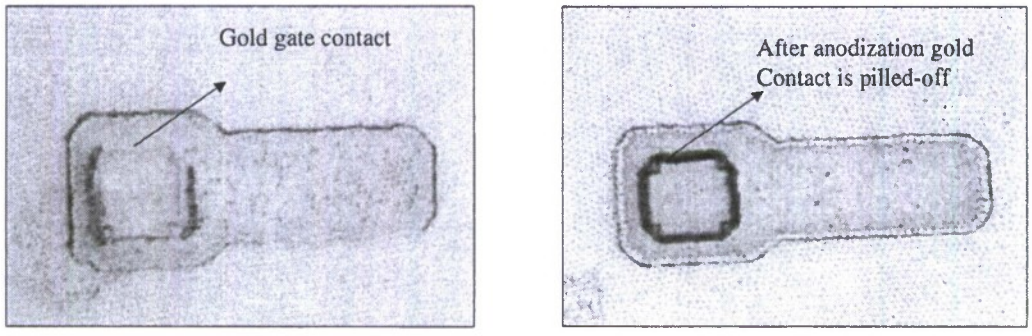

Figure 16 - the gold pad was affected by the anodization

A.3.4. Issue with Reactive Ion etching of injection nano-hole

RIE etching the nanoholes in Al: After anodization of Al to keep the connections isolated, we need to etch the nanoholes to form top contact with the substrate below. It was found to be very difficult to etch the SiO_2 below the nanoholes. There were a lot of possible reasons and conditions to explore. The reason we think was the thin layer of photoresist. After getting a cleaner surface, we showed the etched nanoholes.

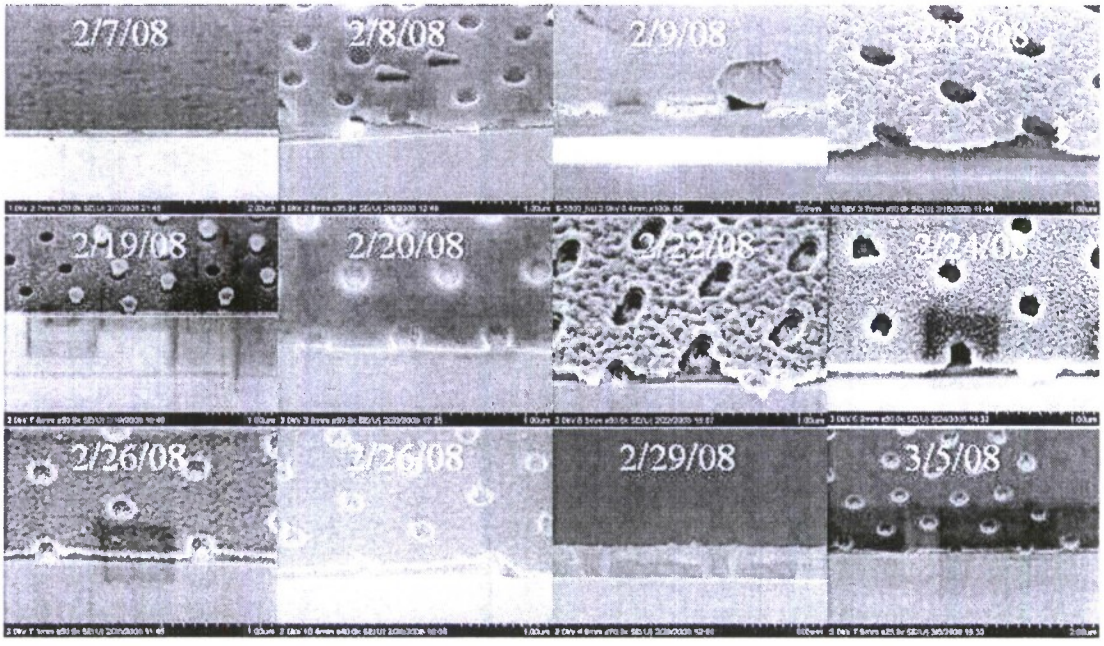

Figure 17 - the evolution of making nanoholes in SiO_2

A.3.5. Lift-off problem

Four of the six photolithography plus the maskless nanolithography techniques are based on the lift-off process. But the lift-off was always very difficult to get the clean surface either in nanoscale or microscale. A clean surface is critically important to get a good electrical contact. So, to avoid so many lift-off processes, we are also developing the metal etching processes, such as Ti, Au and Aluminum. Currently, we had the recipes to quantitatively etch Ti by hot phosphoric acid or buffered HF, Au by the commercial iodine and potassium iodine solution.

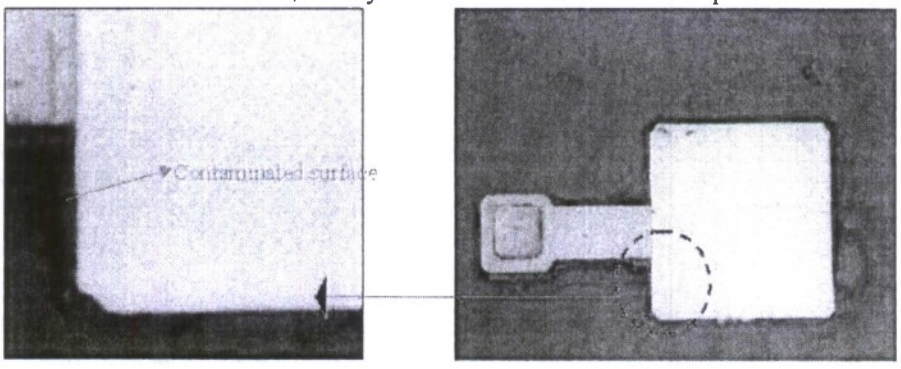

Figure 18 - the edge of the nanopatterns show the photoresist residue

A.3.6. FIB approach

We also implemented an FIB approach to form holes. This method turned out to be expensive, and time consuming.

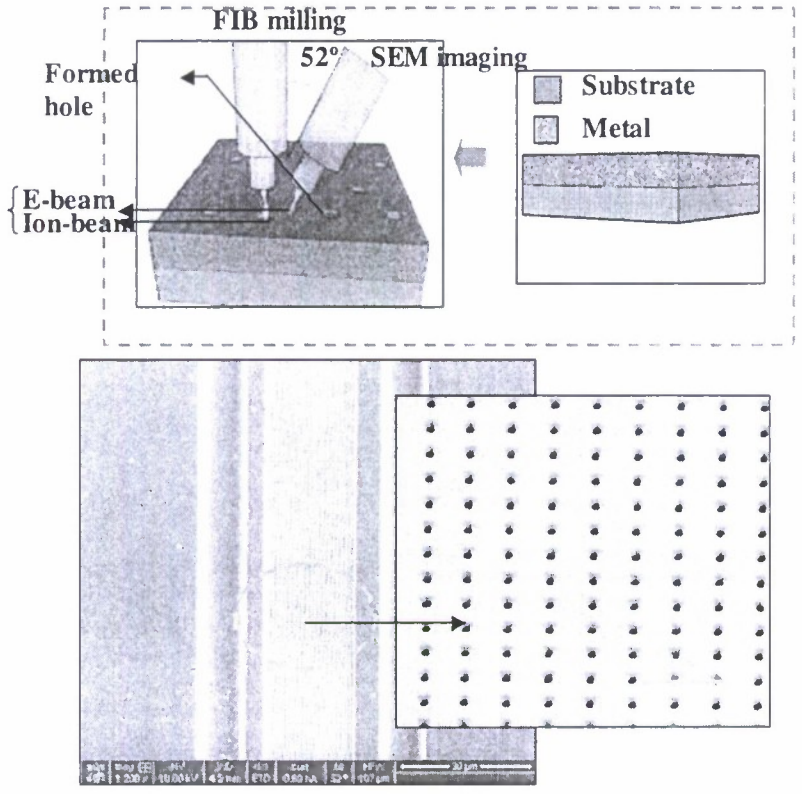

Figure 19 – (a) Schematic diagram showing the FIB process to form the holes (b) SEM image of the holes formed on the ridge using Focused Ion Beam lithography .

A.3.7. E-beam lithography approach

In the beginning of the program we used our used the ebeam facility at Northwestern University to form nanopillar and used lift-off to form the holes. As the resolution of the facility available isn't very high, we couldn't get any holes of size less than 500nm. Any size above 500nm isn't useful for such application, as with wider holes we can't achieve significant electrical confinement. We collaborated with Prof. H. Adesida at University of Illinois at Urbana champagne (UIUC) to form uniform pillars of photoresist with high-resolution ebeam lithographic machine. They took 20 hours to form couple of ridges with uniform pillar. We tried lift-off technique to form holes over the sample but it failed, as the pillar didn't have any under-cut [Figure 20]. The method was extremely expensive and time consuming. We also sent our sample to Air-Force National Laboratory to form photoresist pillars on the ridge, but it took 84 hours of ebeam lithography to finish only a part of the sample. Thus we concentrated more on our technique SLL to form the array of holes, as our method is based on conventional lithography.

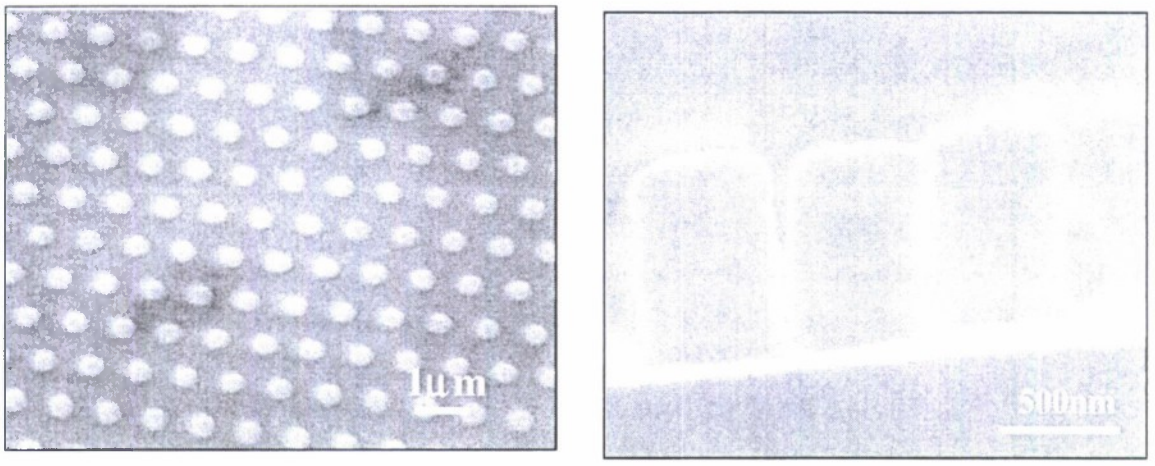

Figure 20 – SEM image showing the formation of nanopillars of photoresist. It was done by the nanotechnology facility at UIUC. The formation of holes by metal lift-off failed as the photoresist nanopillar didn't have any under-cut.

A.3.8. Device structure

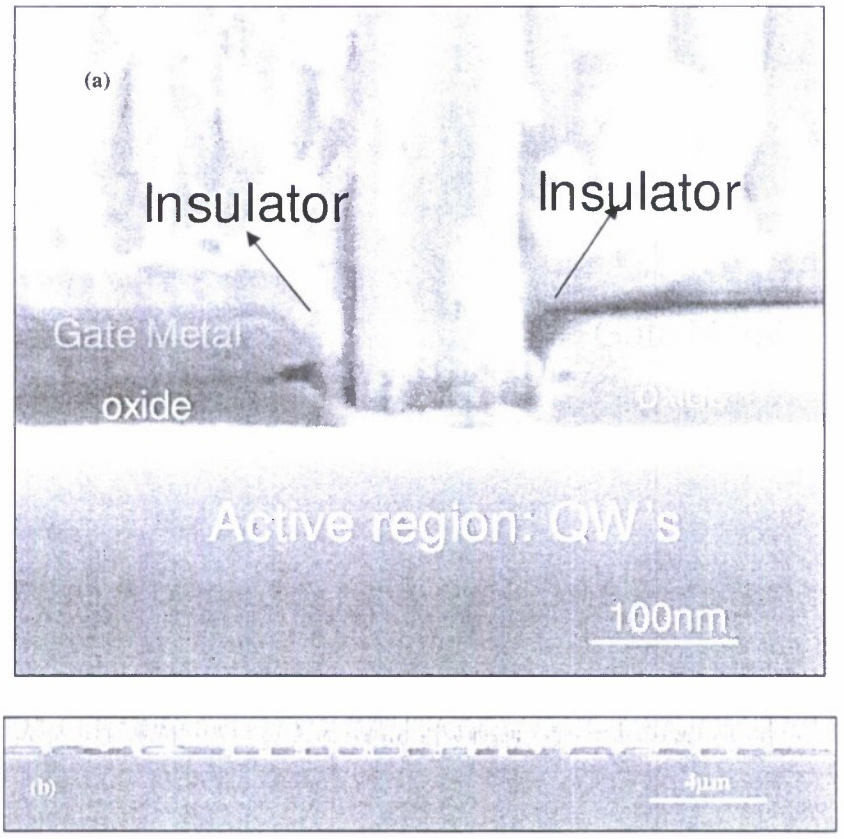

Figure 21 – (a) SEM image of the device with isolated gate and injection contact (b) SEM image showing series of device together.

B.4. Measurement

We designed and put a set-up for current vs voltage (I-V) and current vs power (I-P) measurement for the first time at Bio-inspired sensor and Optoelectronics Laboratory (BISOL), Northwestern University. The set-up uses two parabolic mirrors to collect light using a liquid nitrogen cooled MCT detector. The MCT detector is interfaced with oscilloscope and whole set-up is computer controlled using Labview interface.

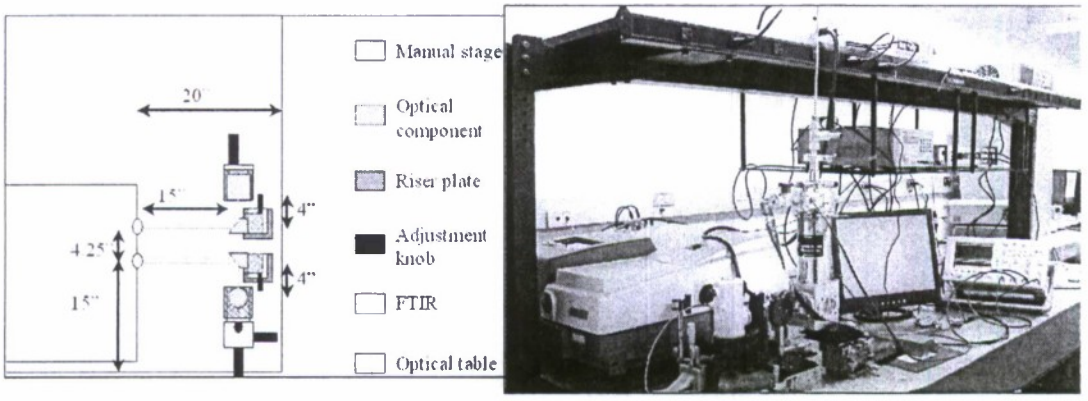

Figure 22 - (a) Design of the I-V-P set-up for characterization of quantum cascade laser (b) Picture showing the lab setup at BISOL.

The output power and applied voltage versus current (L-I-V) characteristics of injectionless Cascade Laser as well with injector QCL were obtained with the mounted device placed on a temperature-controlled cold finger of a nitrogen-cooled cryostat. Power measurements were performed on various laser devices up to 300K, in pulsed mode with a pulse width of 100ns and a repetition frequency of 1KHz. The detector was a liquid nitrogen cooled fast HgCdTe detector with a ~15nsec rise and fall time. Figure 23 shows the L-I-V curve.

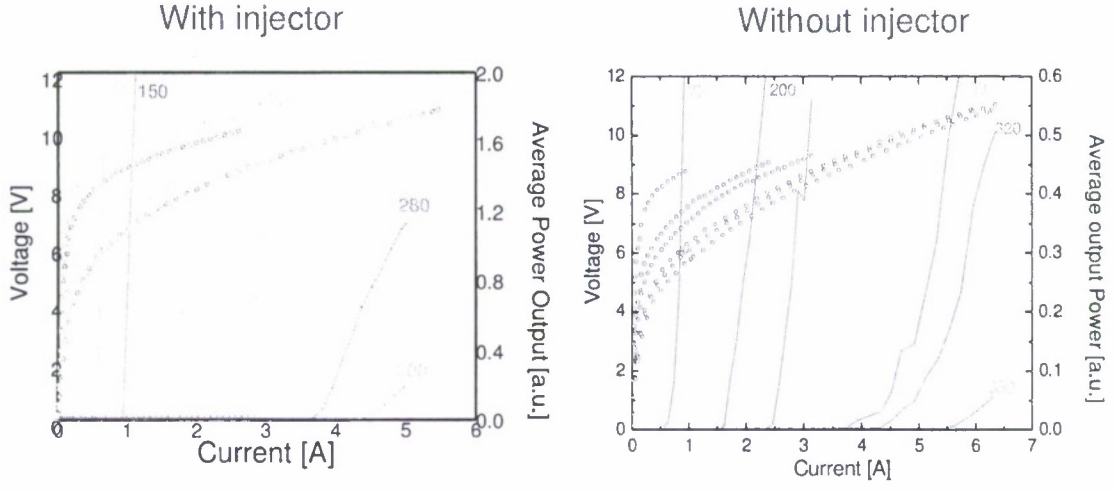

Figure 23 – L-I-V curve for with and without injector cascade laser

Injectorless QCL works at 6.8μm with a threshold current density of 1.1KA/cm^2. Using, I-V data at 77K and assuming that the entire voltage drops occur over the active region only, a voltage defect of as low as 57meV was calculated. This reduction is due to the absence of any doped injector region inside the core laser design where significant voltage drops can occur. Lower voltage defect resists the waste of power as heat, which helps increasing the laser wall-plug efficiency. This result has serious significance in increasing the efficiency of the laser.

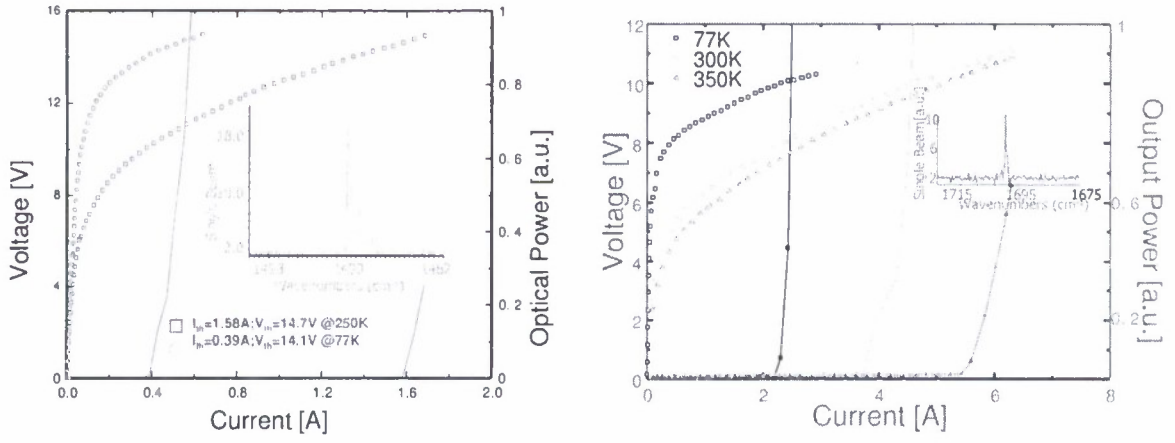

Figure 24 – (a) I-V curve of injectorless QCL showing a voltage defect of ~57meV (b) Using the same measurement set-up, voltage defect of conventional QCL has been measured and it was found to be ~ 120meV at the same temperature of 77K.

Threshold current density, J_{th}, as a function of heat sink temperature has been plotted and fitted with $J_{th}=J_0Exp[T/T_0]$ and it gives a characteristic temperature value of 160K [Figure 25] . Injectorless QC- design also has a reduced optical power loss in the core for free carrier absorption.

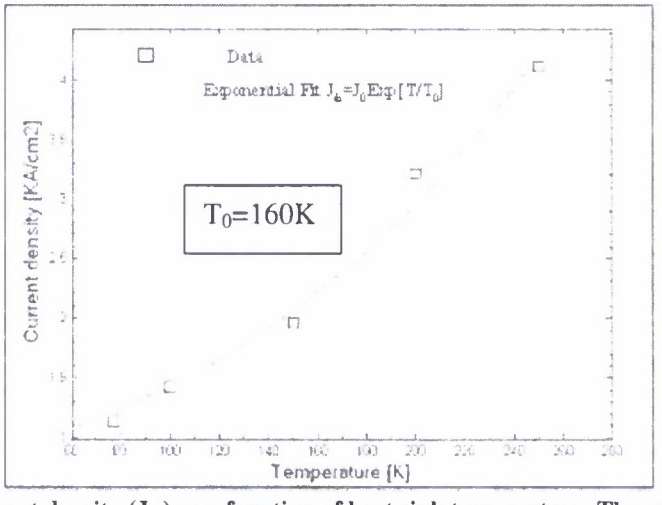

Figure 25 - Pulsed current density (J_{th}) as a function of heat sink temperature. The experimental data were fit with an exponential

We have also designed a set-up to measure the thermal effect on shift of peak wavelength of Quantum Cascade Laser using time resolved step-scan as shown in Figure 26. It shows a shift ~5C over a pulse width of 200ns for QC laser working in 300k.

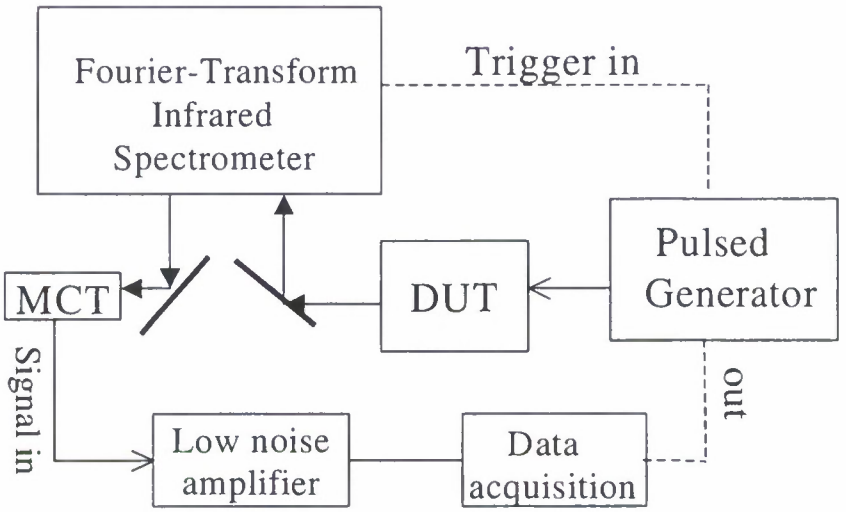

Figure 26 - Schematics of the experimental set-up used to acquire step-scan-time-resolved measurement over the pulse width of 300ns.

The thermal shift was calculated for QCL with and without injector as shown in Figure 27. The injectorless QCL showed a much better performance compared to conventional QCL as it has less number of phonon relaxation happening due to absence of any injectors.

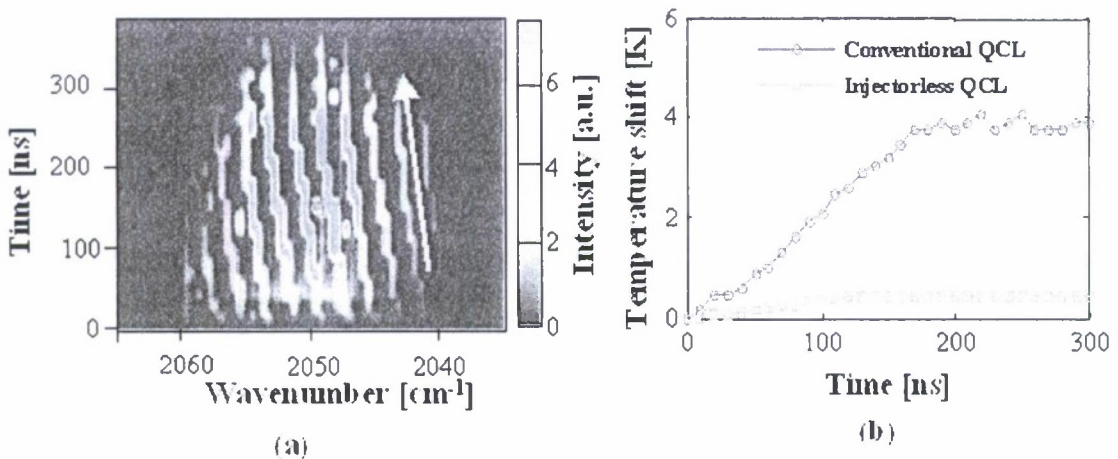

Figure 27 – (a) Thermal shift of wavelength for QCL with injector over a pulse width of 300ns. (b) Comparison of the change in core temperature for QCL with and without injector over a pulse width of 300ns.

PASCAL devices were fabricated as seen from Figure 21. The injection and gate contacts are separated by aluminum oxide of thickness ~ 50nm. The sample has been tested but the electrical insulation wasn't found to be good. A second phase of such sample is under fabrication, which is expected to show stiff insulation and can realize the artificial quantum dot device.